Large Payload Manipulation by Space Robots

Evangelos G. Papadopoulos

Department of Mechanical Engineering &
McGill Research Centre for Intelligent Machines, McGill University
3480 University St., Montreal, PQ, Canada H3A 2A7

Abstract

In this paper, kinematic models for multiple manipulator space robotic systems are developed, as functions of body-fixed barycentric vectors. These models are used to define workspaces for single and multi-manipulator free-floating systems. It is shown that following the capture of a large payload, the location of these workspaces in space changes, and their size is reduced. These effects, common in single and multi-manipulator systems, must be taken into account during planning of manipulation tasks in space. A procedure for manipulating a large payload is proposed. Given a payload and its desired path in space, this procedure yields an optimum grasping posture to ensure successful manipulation of the payload.

I. Introduction

Plans for future space development envisage a broad role for space robotic systems. In-orbit satellites and space structures and stations will require extensive inspection, construction and maintenance capabilities. Astronaut Extra Vehicular Activities (EVA) can be valuable in meeting these requirements. However, the cost of human life support facilities, the limited time available for astronaut EVA, and the high risks involved, make space robotic devices desired astronaut assistants or alternatives. To increase the mobility of such devices, *free-flying* systems in which one or more manipulators are mounted on a thruster-equipped spacecraft, have been proposed [1]. However, extended use of the thrusters severely limits the operational life of free-flyers.

Operation in a *free-floating* mode can increase a system's life [2-5]. In this mode of operation, spacecraft thrusters are turned off, and the spacecraft is permitted to translate and rotate in response to manipulator motions. Additional benefits of this mode of operation include the smoothness of end-effector motions, which is particularly important when manipulating sensitive payloads, and the absence of thruster gases that can disturb satellites, space structures, or cooperating astronauts. Since spacecraft thrusters are not in use during this mode of operation, a free-floating system's linear and angular momentum must be zero to avoid uncontrolled drift or spin. Any accumulated momentum should be removed by a system's reaction wheels and/or thrusters [6,7].

The kinematics and dynamics of free-floating systems can be simplified by the Virtual Manipulator (VM) technique, proposed in [2]. However, a VM for a multiple manipulator system does not result in a minimum parameterization of its kinematics. A Generalized Jacobian for a free-floating system was derived and used to design a resolved-rate type control algorithm [3]. Other control approaches, based on the resolved acceleration, and transposed Jacobian algorithms were proposed [4-5]. It was shown that despite the dynamic coupling between a system's manipulator and its spacecraft, the control of free-floating manipulator is essentially the same as that for a fixed-based system, provided that path-dependent Dynamic Singularities are avoided [6,7]. This can be achieved by restricting the end-effector to move in the Path Independent Workspace (PIW) [6,7]. Some recent works consider dual manipulator systems, and control techniques for the capture of payloads, see for example [8,9].

In this paper, the modeling formulation presented in [6,7] is extended to model multiple manipulator space systems, see Fig. 1.

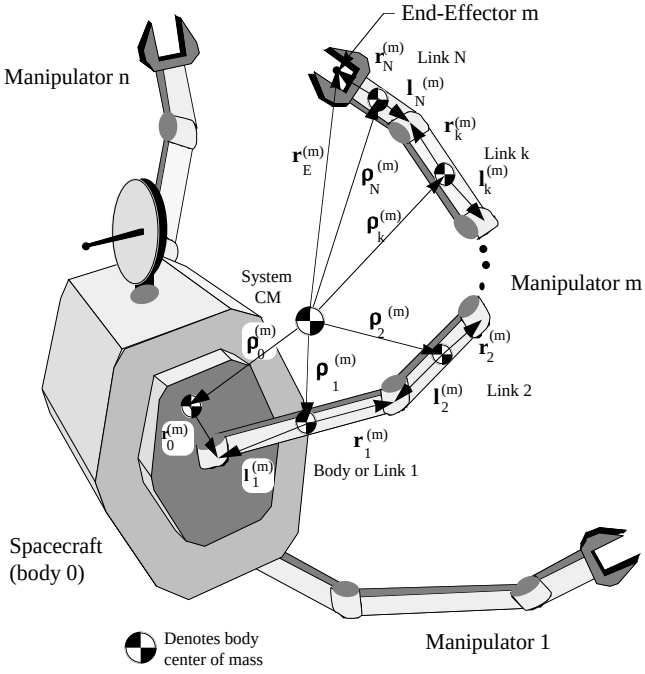

Figure 1. A free-floating space robotic system with n manipulators.

It is shown that the kinematics and dynamics of such systems can be expressed as functions of a set of body-fixed barycentric vectors. The models developed are used in defining workspaces for single and multiple manipulator systems. It is observed that the workspace of some manipulator is affected by the configuration of other system manipulators. The effect of large payloads on a system's workspace is considered. It is shown that free-floating system workspaces shrink as the payload mass and inertia increase. In addition, the location of these workspaces change after the capture of a large payload. These effects occur in single and multiple manipulator systems, and must be taken into account in planning manipulation tasks. Based on this analysis, a large payload manipulation procedure is outlined. Given a payload and its desired path in space, this procedure yields an optimum grasping posture to ensure successful manipulation of the payload.

II. Modeling of Multiple Manipulator Space Robotic Systems

In this section we develop kinematic models for rigid space robotic systems with multiple manipulators. As shown in Figure 1, n manipulators are mounted on a system's spacecraft, represented by body 0. The bodies k (k=1,…,N_m) represent the N_m links of the m^{th} manipulator, (m=1,…,n). Manipulator joint angles and velocities are represented by the $N_m \times 1$ column vectors $\mathbf{q}^{(m)}$ and $\dot{\mathbf{q}}^{(m)}$, (m=1,…,n). The spacecraft can translate and rotate in response to manipulator motions. The manipulators are assumed to have revolute joints and an open-chain kinematic configuration so that a system with N_m Degree-of-Freedom (DOF) manipulators will have 6+N DOFs, where N is given by

$$N = \sum_{m=1}^{n} N_m \qquad (1)$$

Under the assumption of zero external forces, and zero linear momentum, the system Center of Mass (CM) does not move. To simplify the kinematic Eqs., an inertial reference frame is fixed at the system's CM, see Figure 1. Further simplification of these Eqs. occurs by writing the vectors from the system CM to the CM of link k in manipulator m, $\boldsymbol{\rho}_k^{(m)}$, as functions of body-fixed barycentric vectors. This property is similar to that obtained in publications [6,7], in the context of a single manipulator system.

From Figure 1, it can be seen that

$$\begin{aligned}
\boldsymbol{\rho}_k^{(1)} - \boldsymbol{\rho}_{k-1}^{(1)} &= \mathbf{r}_{k-1}^{(1)} - \mathbf{l}_k^{(1)} \qquad k = 1,...,N_1 \\
&\cdots \\
\boldsymbol{\rho}_k^{(m)} - \boldsymbol{\rho}_{k-1}^{(m)} &= \mathbf{r}_{k-1}^{(m)} - \mathbf{l}_k^{(m)} \qquad k = 1,...,N_m \\
&\cdots \\
\boldsymbol{\rho}_k^{(n)} - \boldsymbol{\rho}_{k-1}^{(n)} &= \mathbf{r}_{k-1}^{(n)} - \mathbf{l}_k^{(n)} \qquad k = 1,...,N_n
\end{aligned} \qquad (2)$$

where $\mathbf{r}_k^{(m)}$, and $\mathbf{l}_k^{(m)}$, are the outboard and inboard body-fixed vectors which connect a link's CM to its left and right joints, see Figure 1. Eqs. (2) represent N linear Eqs. with N+1 unknowns. Since $\boldsymbol{\rho}_k^{(i)}$ vectors are defined with respect to the system CM, it holds that

$$m_0\boldsymbol{\rho}_0 + \sum_{m=1}^{n}\sum_{k=1}^{N_i} m_k^{(m)}\boldsymbol{\rho}_k^{(m)} = 0 \qquad (3)$$

Eqs. (2) and (3) are solved for $\boldsymbol{\rho}_k^{(m)}$, and the result is

$$\boldsymbol{\rho}_0 = \mathbf{c}_0^{*} + \sum_{i=1}^{n}\sum_{k=1}^{N_i} \mathbf{l}_k^{*(i)} \qquad (4a)$$

$$\boldsymbol{\rho}_k^{(m)} = \mathbf{r}_0^{*(m)} + \sum_{\substack{i=1 \\ i\neq m}}^{n}\sum_{k=1}^{N_i} \mathbf{l}_k^{*(i)} + \sum_{i=1}^{N_m} \mathbf{v}_{ik}^{(m)} \qquad (4b)$$

where $()_k^*$ is a barycentric vector, fixed in body k. To define them, we first locate the barycenter of each of the system bodies [10]. The barycenter is defined as the center of mass of the original body after adding at each of its joints a point mass equal to the outboard mass from that joint, see Fig. 2.

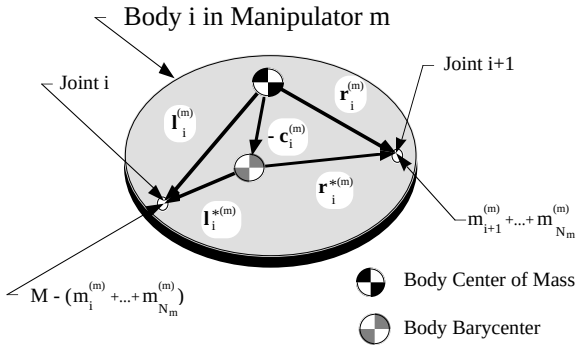

Figure 2. Definition of barycenters and barycentric vectors $\mathbf{l}_i^{*(m)}, \mathbf{c}_i^{*(m)}, \mathbf{r}_i^{*(m)}$.

The location of the N+1 barycenters with respect to the corresponding body CMs are

$$\mathbf{c}_0 = \sum_{i=1}^{n} \mathbf{r}_0^{(i)}\,\mu_1^{*(i)} \qquad (5a)$$

$$\mathbf{c}_i^{(m)} = \mathbf{l}_i^{(m)}\,(1-\mu_i^{*(m)}) + \mathbf{r}_i^{(m)}\,\mu_{i+1}^{*(m)} \qquad i = 1,...,N_m,\ m = 1,\ldots,n \qquad (5b)$$

where $\mu_i^{*(m)}$ is the outboard mass after joint i in manipulator m

$$\mu_i^{*(m)} \equiv \sum_{j=i}^{N_m} \frac{m_j^{(m)}}{M} \qquad i = 0,\ldots,N_m \qquad (6)$$

and M is the total mass of the system

$$M = m_0 + \sum_{i=1}^{n} \sum_{k=1}^{N_i} m_k^{(i)} \tag{7}$$

The barycentric vectors for the spacecraft are given by

$$\mathbf{r}_0^{*(m)} = \mathbf{r}_0^{(m)} - \mathbf{c}_0 \qquad m = 1,\ldots,n \tag{8a}$$

$$\mathbf{c}_0^{*} = -\mathbf{c}_0 \tag{8b}$$

and for link i in manipulator m are given by

$$\mathbf{v}_{ik}^{(m)} \equiv \left\{ \begin{array}{ll} \mathbf{r}_i^{*(m)} = \mathbf{r}_i^{(m)} - \mathbf{c}_i^{(m)} & i<k \\ \mathbf{c}_i^{*(m)} = -\mathbf{c}_i^{(m)} & i=k \\ \mathbf{l}_i^{*(m)} = \mathbf{l}_i^{(m)} - \mathbf{c}_i^{(m)} & i>k \end{array} \right\} \tag{9}$$

Therefore, there exist n+1 vectors for the spacecraft, namely $\mathbf{c}_0^{*}$, and $\mathbf{r}_0^{*(m)}$ (m=1,…n), while for each manipulator link there exist three vectors, namely $\mathbf{r}_i^{*(m)}$, $\mathbf{c}_i^{*(m)}$, and $\mathbf{l}_i^{*(m)}$.

Expressions (4a,b) correspond to a particularly clear physical picture. The N+1 barycentric vectors that form $\boldsymbol{\rho}_k^{(m)}$ are chosen among the $\mathbf{l}_i^{*(j)}$ or $\mathbf{r}_i^{*(j)}$ vectors from each body, so that the chosen vector points towards the closest joint to body k in manipulator m. Body k in manipulator m, is represented in $\boldsymbol{\rho}_k^{(m)}$ by $\mathbf{c}_k^{*(m)}$, see Figure 3. Note that Eq. (4) requires only N+1 barycentric vectors to yield $\boldsymbol{\rho}_k^{(m)}$. In contrast to this, the VM modeling technique would result in a N+n link virtual manipulators with n spherical joints [2]. Therefore, the present formulation corresponds to a minimum kinematic parameterization for $\boldsymbol{\rho}_k^{(m)}$, which is advantageous in the development of Eqs. of motion.

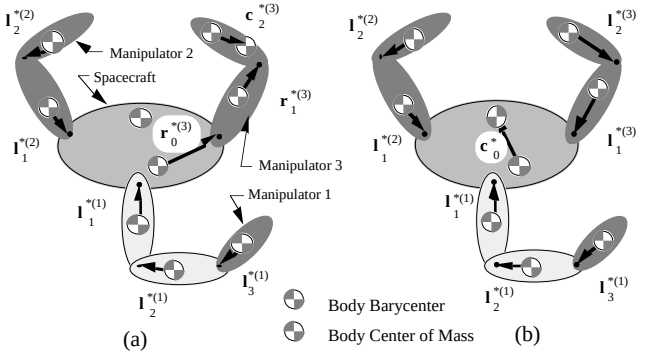

Figure 3. Barycentric vectors that make up (a) $\boldsymbol{\rho}_2^{(3)}$, and (b) $\boldsymbol{\rho}_0$.

Eq. (4b) can be used to find the position of the end-effector of the m^{th} manipulator as

$$\mathbf{r}_E^{(m)} = \boldsymbol{\rho}_N^{(m)} + \mathbf{r}_N^{(m)} \tag{10}$$

Since $\boldsymbol{\rho}_N^{(m)}$ is equal to the sum of N+1 barycentric vectors, each fixed on some body of the system, the motion of the m^{th} end-effector will be affected by the motion of any joint in the system. However, it is expected that some motions will have more prominent effects than others.

Using Eqs. (4), (10), the derivative of $\boldsymbol{\rho}_k^{(m)}$ is written as

$$\dot{\boldsymbol{\rho}}_k^{(m)} = \boldsymbol{\omega}_0^{\times}\mathbf{r}_0^{*(m)} + \sum_{\substack{i=1 \\ i\neq m}}^{n} \sum_{k=1}^{N_i} \boldsymbol{\omega}_k^{(i)\times}\,\mathbf{l}_k^{*(i)} + \sum_{m=1}^{N_m} \boldsymbol{\omega}_k^{(m)\times}\mathbf{v}_{ik}^{(m)} \tag{11}$$

where $\boldsymbol{\omega}_0$ is the angular velocity of the spacecraft, and $\boldsymbol{\omega}_k^{(m)}$ the angular velocity of body k in manipulator m. The symbol $(^{\times})$ operates on a 3×1 vector to create the corresponding cross product skew-symmetric matrix. Following a procedure similar to that in Ref. [7], this result can be used to express compactly the angular momentum of the system, in the spacecraft frame 0:

$${}^0\mathbf{h}_{cm} = {}^0\mathbf{D}\,{}^0\boldsymbol{\omega}_0 + {}^0\mathbf{D}_{\mathbf{q}}\,\dot{\mathbf{q}} = \mathbf{0} \tag{12}$$

where ${}^0\mathbf{D}$ is a 3×3 positive definite matrix, function of the system configuration $\mathbf{q} = [\mathbf{q}^{(1)},\ldots,\mathbf{q}^{(n)}]^T$, ${}^0\mathbf{D}_{\mathbf{q}}$ is a 3×N mixed inertia matrix, also function of $\mathbf{q}$. The system joint rates are $\dot{\mathbf{q}} = [\dot{\mathbf{q}}^{(1)},\ldots,\dot{\mathbf{q}}^{(n)}]^T$. Both ${}^0\mathbf{D}$ and ${}^0\mathbf{D}_{\mathbf{q}}$ can be written using the barycentric vectors.

The end-effector velocities given by the 1×6n vector $\boldsymbol{V}_E$

$$\boldsymbol{V}_E = [\,\mathbf{v}_E^{(1)}, \boldsymbol{\omega}_E^{(1)},\ldots,\mathbf{v}_E^{(n)}, \boldsymbol{\omega}_E^{(n)}]^T \tag{13}$$

depend on the angular velocity of the spacecraft and on all joint rates $\dot{\mathbf{q}}$. Using the angular momentum Eq., we can express the spacecraft angular velocity ${}^0\boldsymbol{\omega}_0$ as a function of the joint rates $\dot{\mathbf{q}}$, and subsequently eliminate it from the expressions for $\boldsymbol{V}_E$. Therefore, $\boldsymbol{V}_E$ is related to the joint rates $\dot{\mathbf{q}}$ according to

$$\boldsymbol{V}_E = \mathrm{diag}(\mathbf{T}_0,\ldots,\mathbf{T}_0)\;{}^0\mathbf{J}^{*}(\mathbf{q})\,\dot{\mathbf{q}} \tag{14}$$

where $\mathbf{T}_0$ is the 3×3 spacecraft orientation matrix, and ${}^0\mathbf{J}^{*}(\mathbf{q})$ is a 6n×N Jacobian matrix, function of the system mass properties and configuration $\mathbf{q}$. If all manipulators have 6 DOF, this Jacobian is square. As pointed out in [6,7], there exist system configurations $\mathbf{q}$ at which ${}^0\mathbf{J}^{*}(\mathbf{q})$ is deficient, or singular. These configurations give rise to *dynamic singularities* which are fixed in a system's joint space, but their existence in Cartesian space depends on the path taken to reach a particular location. Briefly, this is due to the nonintegrability of the angular momentum, see Eq. (12), [6,7]. These characteristics apply in the case of multiple manipulators, too. Next, based on the developed kinematic models, we study some important workspaces for multiple manipulator systems.

III. Workspaces of Multiple Manipulator Space Robots

An important workspace for any robotic system is its *reachable workspace*. It is well known that the reachable workspace of a single-manipulator free-floating system, is contained in a spherical volume centered at the system CM, [2,6]. In a multi-manipulator free-floating system, each manipulator has its own reachable workspace. Since the distance from the system CM to the m^{th} end-effector is invariant with respect to the spacecraft's orientation, its reachable workspace is a hollow sphere centered at the system CM, and contained within the spherical shells with radii

$$R_{min}^{(m)} = \min_{\mathbf{q}} \|\mathbf{r}_E^{(m)}\| \qquad m = 1,\ldots,n \qquad (15a)$$

$$R_{max}^{(m)} = \max_{\mathbf{q}} \|\mathbf{r}_E^{(m)}\| \qquad m = 1,\ldots,n \qquad (15b)$$

where $\mathbf{r}_E^{(m)}$ is given by Eq. (10), and the symbol $\|\bullet\|$ denotes the length of vector $(\bullet)$. If joint limits are taken into account, then this workspace will be reduced further. However, note that in order for the m^{th} end-effector to be at a specific location, other manipulators may have to assume particular configurations. For example, in a two manipulator system, in order for end-effector 1 to be at $R_{max}^{(1)}$, the second manipulator must be fully extended in a direction opposite to manipulator 1.

For the above reason, it is useful to define a workspace which contains all the points that can be reached by an end-effector irrespective of the configuration of other system manipulators. Such a workspace, called here the *Guaranteed Workspace*[1](GW), is contained in the spherical shells with radii

$$R'^{(m)}_{max} = \Big| - \max_{\substack{\mathbf{q}(i) \\ i\neq m}} \Big\| \mathbf{r}_0^{*(m)} + \sum_{\substack{i=1 \\ i\neq m}}^{n} \sum_{k=1}^{N_i} \mathbf{l}_k^{*(i)} \Big\| + \max_{\mathbf{q}(m)} \Big\| \mathbf{r}_N^{(m)} + \sum_{i=1}^{N_m} \mathbf{v}_{ik}^{(m)} \Big\| \Big| \qquad (16a)$$

$$R'^{(m)}_{min} = \Big| + \max_{\substack{\mathbf{q}(i) \\ i\neq m}} \Big\| \mathbf{r}_0^{*(m)} + \sum_{\substack{i=1 \\ i\neq m}}^{n} \sum_{k=1}^{N_i} \mathbf{l}_k^{*(i)} \Big\| + \min_{\mathbf{q}(m)} \Big\| \mathbf{r}_N^{(m)} + \sum_{i=1}^{N_m} \mathbf{v}_{ik}^{(m)} \Big\| \Big| \qquad (16b)$$

and is a subset of the reachable workspace. In defining $R'^{(m)}_{max}$, the first term to be maximized represents the effect of the spacecraft and all the manipulators, except the m^{th} one, while the second one represents the effect of the m^{th} manipulator. Hence, Eq. (16a) gives the maximum distance at which the m^{th} end-effector can be, when the rest of the system is in its worse configuration with respect to the m^{th} end-effector's reachability. $R'^{(m)}_{min}$ is defined similarly.

The Guaranteed Workspace is particularly useful in multi-manipulator systems, because it represents the Cartesian space that an end-effector can reach, without need for cooperation from other manipulators, or without employing a spacecraft's thrusters. If the m^{th} end-effector is at a location in its GW then, when other manipulators move, its manipulator can always take corrective action to keep it at the initial location. Depending on the mass distribution of a system, one or more manipulators may lack a GW. This can occur when the m^{th} end-effector is affected more by the motion of some other manipulator, than by the motion of its own one. Typically, this is the case when some manipulator grabs a very large payload.

Another important workspace for free-floating systems is the Path Independent Workspace (PIW), defined for a single manipulator system in [6]. This is the volume free of dynamic singularities, and is obtained by excluding all the points which can be reached in a singular configuration $\mathbf{q}_S$. To reach points in the PIW, any path can be used. The workspace in which dynamic singularities may occur is called the Path Dependent Workspace (PDW). To reach points in this workspace, carefully selected paths must be used.

PIWs can be defined for multi-manipulator systems, as the volume in space in which the end-effectors can move without going through a dynamic singularity. For a system with 6 DOF manipulators, the singular configurations $\mathbf{q}_S$ are found from

$$\det[{}^0\mathbf{J}^*(\mathbf{q}_S)] = 0 \qquad (17)$$

where ${}^0\mathbf{J}^*$ is given by Eq. (14). The computation of the PIW is not an easy task, since it requires solving complex transcendental Eqs.. However, it can be shown by example that the PIW for a single manipulator is a subset of its GW, defined by Eqs. (16). Since the definition of the GW requires kinematic calculations only, one can use the GW instead of the PIW as a first approximation.

As an example, the workspace limits for the two-manipulator system depicted in Figure 4, are computed. The system geometric and mass properties are given in Table I.

Table Ia. Spacecraft parameters, see Fig. 4.

Body	$r_0^{(1)}$ (m)	$r_0^{(2)}$ (m)	m_0 (kg)	I_0 (Kgm^2)
0	0.5	0.5	400	66.67

Table Ib. Manipulator parameters, see Fig. 4.

[1] For a single manipulator system, this workspace becomes identical to the *Free Workspace*, defined in Ref. [2], or the *Guaranteed Workspace*, defined in Ref. [11].

m	Body k	$l_i^{km)}$ (m)	$r_k^{(m)}$ (m)	$m_k^{(m)}$ (Kg)	$I_k^{(m)}$ (Kgm^2)
1	1	0.5	0.5	40	3.33
1	2	0.5	0.5	30	2.5
2	1	0.5	0.5	40	3.33
2	2	0.5	0.5	30	2.5

For this system, Eq. (10) yields the position of the two end-effectors as

$$x_E^{(m)} = \alpha^{(m)}\cos(\theta) + \beta^{(m)}\cos(\theta+q_1^{(1)}) + \gamma^{(m)}\cos(\theta+q_1^{(1)}+q_2^{(1)}) + \delta^{(m)}\cos(\theta+q_1^{(2)}) + \varepsilon^{(m)}\cos(\theta+q_1^{(2)}+q_2^{(2)}) \qquad m = 1,2 \qquad (18a)$$

$$y_E^{(m)} = \alpha^{(m)}\sin(\theta) + \beta^{(m)}\sin(\theta+q_1^{(1)}) + \gamma^{(m)}\sin(\theta+q_1^{(1)}+q_2^{(1)}) + \delta^{(m)}\sin(\theta+q_1^{(2)}) + \varepsilon^{(m)}\sin(\theta+q_1^{(2)}+q_2^{(2)}) \qquad m = 1,2 \qquad (18b)$$

The angles θ, and $q_k^{(m)}$, are the spacecraft orientation, and the k^{th} joint angle in the m^{th} manipulator. The magnitude of the coefficients α-ε correspond to lengths of system barycentric vectors, i.e., $|\alpha^{(m)}| = \|\mathbf{r}_0^{*(m)}\|$, etc. The values of these coefficients are displayed in Table II. The reachable and the Guaranteed Workspace limits for each manipulator are found using Eqs. (15) and (16), and the results are displayed in Table III, and depicted in Figure 4. Note that due to the symmetry of this system, the two manipulators have identical workspaces. Their GWs are much smaller than their reachable workspace.

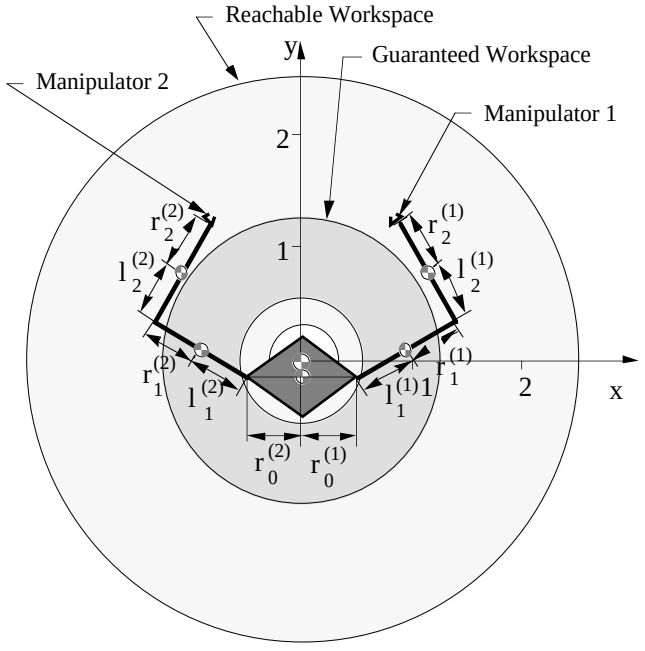

Figure 4. Reachable and Guaranteed Workspaces for a two manipulator system.

In the next section, we examine the effect of payloads on a free-floating system's workspaces.

Table II. Coefficients $\alpha-\varepsilon$, (no payload).

m	$\alpha^{(m)}$	$\beta^{(m)}$	$\gamma^{(m)}$	$\delta^{(m)}$	$\varepsilon^{(m)}$
1	0.5	0.907	0.972	-0.093	-0.028
2	-0.5	-0.093	-0.028	0.907	0.972

Table III. Workspace limits, (no payload).

m	$R_{max}^{(m)}$	$R_{min}^{(m)}$	$R'^{(m)}_{max}$	$R'^{(m)}_{max}$
1	2.50	0.314	1.258	0.686
2	2.50	0.314	1.258	0.686

IV. Effects of Large Payloads on a System's Workspace

Future missions will require motion of large payloads in Cartesian space. EVA astronauts may not be able to manipulate such payloads due to physical limitations; space robots can be used instead. Payload manipulation in Cartesian space will be important especially during cooperation of space robots, or assembly of space structures, etc. The payloads may have large mass and inertia, approaching the mass and inertia of the space robot itself. Therefore, it is important to analyze the effect of grabbing a payload on system workspaces.

As was shown above, the size of a system's reachable workspace depends on a set of barycentric vectors, see Eqs. (10) and (15). Also, Eqs. (4), (5), and (8), indicate that all barycentric vectors are functions of the mass distribution, as described by $\mu_i^{*(m)}$. When a payload is grabbed by the m^{th} end-effector, the mass distribution changes. Assuming a rigid grasp, the payload becomes part of the last link of the m^{th} manipulator, and the location of the center of mass of that link changes. The total system mass, M, is increased by the mass of the payload, m_p, and the system CM moves toward the payload. Since m_p appears as an outboard mass for the m^{th} manipulator, all body barycenters will move towards the body joint which is closest to the payload. The result is a reduction in the length of all the barycentric vectors $\mathbf{l}_k^{*(i)}$ ($i=1,\ldots,n$, $i\neq m$, $k=1,\ldots,N_i$), $\mathbf{r}_0^{*(m)}$, and of all $\mathbf{r}_l^{*(m)}$ ($l=1,\ldots,N_m$). Therefore, the size of the reachable workspace of the m^{th} manipulator is reduced. The workspace of the other manipulators may increase or decrease, depending on the mass distribution. Usually, the size of these other workspaces will increase.

As an example, assume that manipulator 1 of the system shown in Figure 4 grabs a stationary payload of mass m_p =

400kg, at the payload's CM, called CM_p. The new coefficients in Eqs. (18) are displayed in Table IV, and the new workspace limits, in Table V. As predicted, the radius of the reachable workspace for manipulator 1 decreased from 2.50m to 1.437m, while the radius of the second manipulator's reachable workspace increased to 3.613m. Although this workspace has increased substantially, in order to realize it, manipulator 1 has to assume a favorable configuration (fully extended). Similarly, the first manipulator's GW is decreased. However, the second manipulator's GW vanishes, meaning that there are no points that this manipulator can reach irrespective of where the first one is. Therefore, to allow manipulator 2 reach a given point, cooperation of manipulator 1 may be required.

Table IV. Coefficients $\alpha-\varepsilon$, (with payload).

m	$\alpha^{(m)}$	$\beta^{(m)}$	$\gamma^{(m)}$	$\delta^{(m)}$	$\varepsilon^{(m)}$
1	0.287	0.522	0.559	-0.053	-0.016
2	-0.713	-0.478	-0.491	0.947	0.984

Table V. Workspace limits, (with payload).

m	$R_{max}^{(m)}$	$R_{min}^{(m)}$	$R'_{max}^{(m)}$	$R'_{max}^{(m)}$
1	1.437	0.181	0.725	0.393
2	3.613	0.219	n/a	n/a

An additional effect of grabbing a payload is that the system CM moves towards the payload, on a line that connects the system CM before capture to CM_p. After the capture of a payload, the end-effector may be located in an unfavorable part of its workspace, i.e. outside its GW or PIW. In such a case, attempts to move the payload along some desired path may require cooperation from other manipulators, or may fail due to the occurrence of dynamic singularities. In the next section we present a procedure which ensures successful manipulation of a payload.

V. Manipulation of Large Payloads

Payload manipulation by a free-flying space robot can occur according to the following scenario. The payload is located at some given point and must be moved along a given path in Cartesian space. A free-flyer is commanded to approach the payload, in an appropriate configuration, and grab it. During the approach phase, the free-flyer will be using its jet thrusters, and can be controlled according to various free-flying control strategies, see for example Refs. [12,13]. Just before grabbing the payload, the free-flyer turns off its thrusters to avoid disturbing the payload, and operates in a free-floating mode. Following capture, the payload is moved along the given Cartesian path. To implement the above scenario, a planner would need to know two key elements: (a) how close to the target payload a free-flyer should move, and (b) which configuration the free-flyer should have before capture. This is studied below.

As discussed in the previous section, the size of a manipulator's workspaces is reduced after capture, and the system CM moves towards the payload's CM_p. Just before, during, and just after capture, the end-effector remains at the same Cartesian location. If the desired path happens to be outside the manipulator's post capture GW or PIW, then the end-effector will not be able to move the payload without assistance from other manipulators, or from the spacecraft thrusters. Therefore, the desired path should be in the post capture GW, or preferably, in the PIW of the payload carrying manipulator.

To simplify the analysis, we assume that the end-effector grabs the payload at its CM_p. If the payload mass and inertia properties are known, the PIW can be found by excluding from the reachable workspace all locations that may be reached in singular configurations, [6]. Note that most objects of interest in space are man-made and therefore, they have precisely known properties. To ensure successful manipulation, the PIW must be positioned in Cartesian space such that the desired path fits in it. Locating the post-capture PIW in Cartesian space, also locates the CM of the robot/payload system, denoted by CM_+. Just after capture, the distance of the end-effector from CM_+, R_+, is also known since it is the distance of the beginning of the given path from CM_+. As noted above, the CM of the free-flyer before capture must lie on the line connecting CM_p and CM_+, see Figure 5. Therefore, the pre-capture distance of the free-flyer's CM from the payload, called here *approach distance* R, is given by

$$R = \frac{M+m_p}{M} R_+ \tag{19}$$

where M is the free-flyer mass, and m_p the mass of the payload. In other words, Eq. (19) dictates that just before capture, the CM of the free-flyer must be at the approach distance R from the payload in order to be able to move it along the specified path successfully.

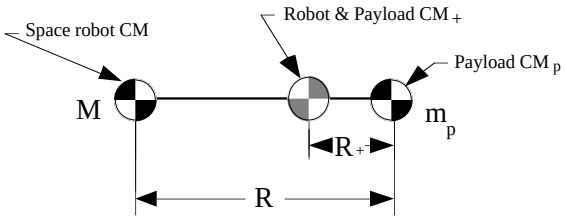

Figure 5. The position of the CM_+ of the combined robot/payload system.

If the path can not fit in the PIW, but can fit in the reachable workspace, then the manipulator may not be able to move the payload along the specified path, due to the existence of dynamic singularities. Then, either the system's

thrusters should be used, or a special path in Cartesian space should be employed, see [13]. If the path cannot be fitted in the reachable workspace, then the system's thrusters will have to be used.

Finding the location of the system CM before capture is not enough to specify the initial spacecraft orientation, $\boldsymbol{\Theta}$, and manipulator configuration, $\mathbf{q}$, because a particular location in Cartesian space can be reached by an infinite number of sets ($\boldsymbol{\Theta}$, $\mathbf{q}$). This additional freedom can be used to optimize a certain criterion, for example optimize a system's configuration to be as much as possible away from singularities. Using such a criterion will result in an optimum capture set ($\boldsymbol{\Theta}$, $\mathbf{q}$).

The above procedure specifies both how close a free-flyer should come to a target, as well as its configuration at capture. As an example, we consider again the free-flyer whose properties are given in Table I, but with manipulator 2 missing. The superscripts are dropped for brevity. The mass of the payload is m_p = 400kg, and its inertia about its CM_p, I_p = 25kgm^2. The position of the end-effector in inertial space is given by

$$x_E = \alpha\cos(\theta) + \beta\cos(\theta+q_1) + \gamma\cos(\theta+q_1+q_2) \qquad (20a)$$

$$y_E = \alpha\sin(\theta) + \beta\sin(\theta+q_1) + \gamma\sin(\theta+q_1+q_2) \qquad (20b)$$

where the values of α, β, and γ after capture are α = 0.230m, β = 0.483m, γ = 0.523m. The workspace limits for the combined robot/payload system are given in Table VI. The desired path for the payload is straight line AB of length 0.25m. For this path, the post capture PIW is located in Cartesian space so that AB lies entirely in it, see Figure 7. As a result, CM_+ is placed at R_+ = 0.540m from point A, with (CM_+)A perpendicular to AB. Eq. (19) yields the approach distance as R = 1m.

Next, an appropriate capture configuration $\mathbf{q} = [q_1, q_2]^T$, and spacecraft orientation, θ, are selected. To this end we choose to maximize the determinant of the post capture system Jacobian, under the constraint that the end-effector is at distance R_+ from the CM_+. The rationale for this choice is that the greater the value of this determinant is, the less likely it is for the system to be in a singular configuration, when the end-effector moves outside the PIW. R_+ can be expressed as a function of $\mathbf{q}$ by

$$R_+ = 0.540 = \sqrt{x_E^2+y_E^2} =$$

$$= \sqrt{\alpha^2+\beta^2+\gamma^2+2\alpha\beta\cos(q_1)+2\alpha\gamma\cos(q_1+q_2)+2\beta\gamma\cos(q_2)} \qquad (21)$$

Eq. (21) is solved for q_2, to yield two families of solutions, see Figure 6. Figure 6 also shows the corresponding families for the determinant $\det[{}^0\mathbf{J}^*(\mathbf{q})]$.

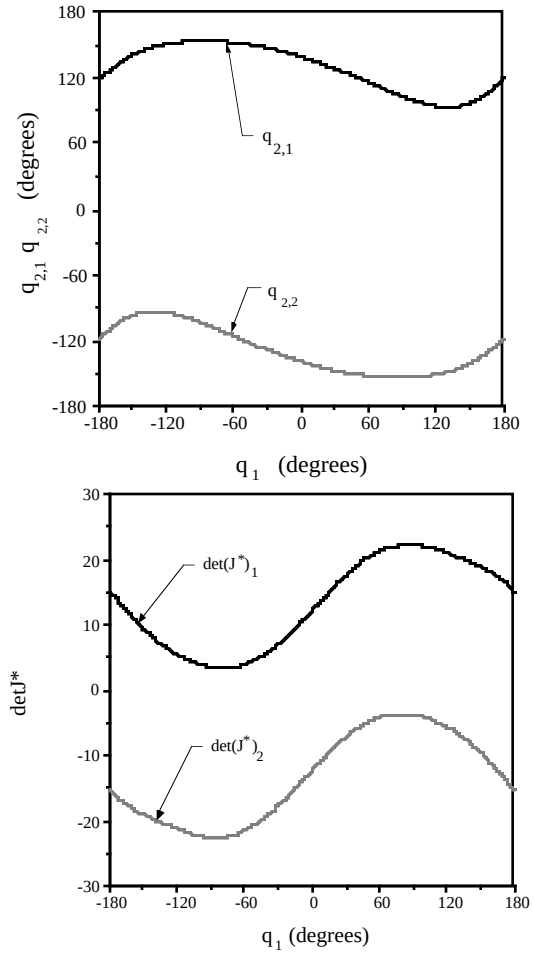

Figure 6. Configurations $q_2(q_1)$ and $\det(J^*(q))$ which correspond to point A at Fig. 7 (capture of the payload).

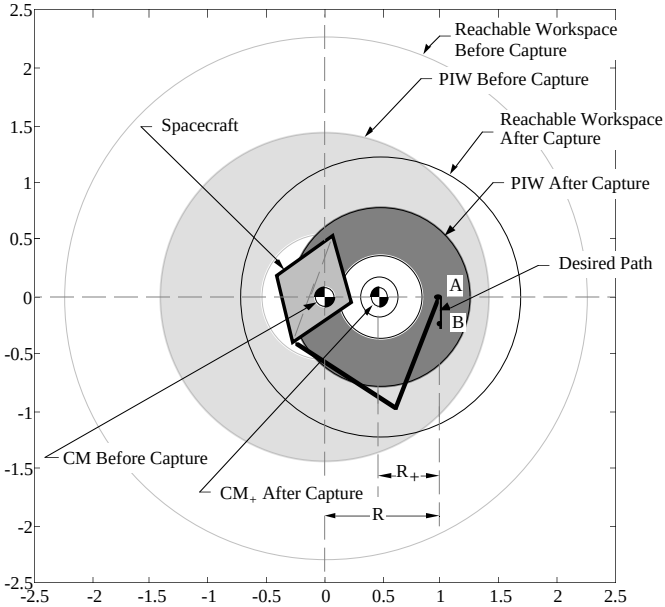

Figure 7. The workspaces before and after the capture of a payload at A. The payload desired path after capture is AB. Also shown is the optimum space robot configuration during capture of a payload (not shown).

Table VI. Workspace limits for the robot / payload system in Fig. 7.

R_{max}	R_{min}	R_{PIWmax}	R_{PIWmin}	R'_{max}	R'_{min}
1.236	0.190	0.776	0.370	0.776	0.270

Figure 6 shows that the determinant is maximized at $q_1 = \pm 79°$. Choosing the positive value, Eq. (21) yields $q_2 = 97.97°$. The orientation of the spacecraft θ can be found by setting in Eqs. (20), $x_E = 0.540$, $y_E = 0$, $q_1 = 79°$, $q_2 = 97.97°$. The result is $\theta = -109°$. Therefore, in order to move the payload along the path AB, the free-flyer must approach its CM at a distance R = 1m from it, at a system configuration and spacecraft orientation, $[\theta, q_1, q_2]^T = [-109°, 79°, 97.97°]^T$. This completes the procedure. The posture of the free-flyer in space is depicted in Figure 7.

VI. Conclusions

In this paper, kinematic models for multiple manipulator space robot systems were presented, and were shown to be functions of body-fixed barycentric vectors. The models developed were used to define workspaces for single and multiple manipulator systems. The effect of large payloads on a system's workspaces was considered next. It was shown that free-floating system workspaces shrink as the payload mass increases. In addition, the location of these workspaces changes after capture of a large payload. These effects occur in single and multiple manipulator systems, and must be taken into account in planning manipulation tasks. Based on the this analysis, a procedure for the manipulation of large payloads was presented. Given a payload and a desired Cartesian path, this procedure suggests an optimum grasping posture which guarantees successful manipulation of the payload.

VII. Acknowledgments

The support of this work by the Natural Sciences and Engineering Council of Canada (NSERC) and by the McGill Faculty of Graduate Studies and Research is gratefully acknowledged.

VIII. References

[1] Bronez, M. A., et al., "Requirements Development for a Free-Flying Robot - the ROBIN," *Proc. IEEE Int. Conf. on Robotics and Automation*, San Fransisco, CA, April 1986.

[2] Vafa, Z. and Dubowsky, S., "On the Dynamics of Space Manipulators Using the Virtual Manipulator, with Applications to Path Planning," *J. Astr. Sciences*, Vol. 38, No. 4, 1990, pp. 441-472.

[3] Umetani, Y. and Yoshida, K., "Resolved Motion Control of Space Manipulators with Generalized Jacobian Matrix," *IEEE Trans. on Robotics and Automation*, Vol. 5, No. 3, 1989, pp. 303-314.

[4] Alexander, H. and Cannon, R., "Experiments on the Control of a Satellite Manipulator," *Proc. 1987 American Control Conf.*, Seattle, WA, June 1987.

[5] Masutani, Y., Miyazaki, F., and Arimoto, S., "Sensory Feedback Control for Space Manipulators," *Proc. IEEE Int. Conf. on Robotics & Automation*, Scottsdale, AZ, May 1989.

[6] Papadopoulos, E. and Dubowsky, S., "Dynamic Singularities in the Control of Free-Floating Space Manipulators," *ASME Journal of Dynamic Systems, Measurement and Control*, Vol. 115, No. 1, March 1993, pp. 44-52. Also in *Space Robotics: Dynamics and Control*, Y. Xu, and T. Kanade eds., Kluwer, Boston, MA, 1993, pp. 77-100.

[7] Papadopoulos, E. and Dubowsky, S., "On the Nature of Control Algorithms for Free-floating Space Manipulators," *IEEE Trans. on Robotics and Automation*, Vol. 7, No. 6, Dec. 1991, pp. 750-758.

[8] Yoshida, K., Kurazume, R., and Umetani, Y., "Dual Arm Coordination in Space Free-flying Robot," *Proc. IEEE Int. Conf. on Robotics and Automation*, Sacramento, CA, April 1991.

[9] Fujii, H., et al., "Capture Control for Manipulator Arm of Free-flying Space Robot," *AIAA Paper*, AIAA-90-3432-CP, 1990.

[10] Wittenburg, J., *Dynamics of Rigid Bodies*, B.G. Teubner, Stuttgart, 1977.

[11] Yoshida, K. and Umetani, Y., "Control of Space Manipulators With Generalized Jacobian Matrix," in *Space Robotics: Dynamics and Control*, Y. Xu, and T. Kanade eds., Kluwer, Boston, MA, 1993, pp. 165-204.

[12] Spofford, J.R. and Akin, D.L., "Redundancy Control of a Free-Flying Telerobot," *Proc. AIAA Guidance, Navigation and Control Conf.*, Minneapolis, MN, August 1988.

[13] Papadopoulos, E. and Dubowsky, S., "Coordinated Manipulator/Spacecraft Motion Control for Space Robotic Systems," *Proc. of the IEEE Int. Conf. on Robotics and Automation*, Sacramento, CA, April 1991, pp. 1696-1701.

[14] Papadopoulos, E., "Path Planning for Space Manipulators Exhibiting Nonholonomic Behavior," *Proc. of the Int. Conf. on Intelligent Robots and Systems*, Raleigh, NC, July 7-10, 1992, pp. 669-675.